Supporting Information

In vivo imaging of histone deacetylases (HDACs) in the central nervous system and major peripheral organs

Changning Wang[1], Frederick A. Schroeder[1, 2], Hsiao-Ying Wey[1], Ronald Borra[1], Florence F. Wagner[3], Surya Reis[2], Sung Won Kim[4], Stephen J. Haggarty[2], Edward B. Holson[3], Jacob M. Hooker[1,*]

[1] Athinoula A. Martinos Center for Biomedical Imaging, Department of Radiology, Massachusetts General Hospital, Harvard Medical School, Charlestown, Massachusetts, 02129

[2] Chemical Neurobiology Laboratory, Departments of Neurology and Psychiatry, Center for Human Genetic Research, Massachusetts General Hospital, 185 Cambridge Street, Boston, Massachusetts, 02114

[3] Stanley Center for Psychiatric Research, Broad Institute of Harvard and MIT, 7 Cambridge Center, Cambridge, Massachusetts, 02142

[4] Laboratory of Neuroimaging, National Institute on Alcohol Abuse and Alcoholism, Bethesda, MD 20892

Table of Contents

Table S1: Screening of **6** against 80 common CNS drug targets and 4 zinc-dependent enzymes reveals limited off-target binding.

Receptor Assay	% Inhibition of Control Specific Binding	Reference Compounds
A1 (h) (antagonist radioligand)	5	DPCPX
A2A (h) (agonist radioligand)	16	NECA
A3 (h) (agonist radioligand)	15	IB-MECA
alpha 1 (non-selective) (antagonist radioligand)	-2	prazosin
alpha 2 (non-selective) (antagonist radioligand)	-7	yohimbine
beta 1 (h) (agonist radioligand)	-11	atenolol
beta 2 (h) (agonist radioligand)	0	ICI 118551
AT1 (h) (antagonist radioligand)	0	saralasin
AT2 (h) (agonist radioligand)	45	angiotensin-II
BZD (central) (agonist radioligand)	-17	diazepam
BZD (peripheral) (antagonist radioligand)	4	PK 11195
BB (non-selective) (agonist radioligand)	-16	bombesin
B2 (h) (agonist radioligand)	6	NPC 567
CGRP (h) (agonist radioligand)	-8	hCGRPalpha
CB1 (h) (agonist radioligand)	17	CP 55940
CCK1 (CCKA) (h) (agonist radioligand)	0	CCK-8s
CCK2 (CCKB) (h) (agonist radioligand)	-8	CCK-8s
D1 (h) (antagonist radioligand)	-4	SCH 23390
D2S (h) (antagonist radioligand)	17	(+)butaclamol
D3 (h) (antagonist radioligand)	-8	(+)butaclamol
D4.4 (h) (antagonist radioligand)	-4	clozapine
D5 (h) (antagonist radioligand)	-1	SCH 23390
ETA (h) (agonist radioligand)	-8	endothelin-1
ETB (h) (agonist radioligand)	-5	endothelin-3
GABA (non-selective) (agonist radioligand)	6	GABA
GAL1 (h) (agonist radioligand)	-9	galanin
GAL2 (h) (agonist radioligand)	1	galanin
PDGF (agonist radioligand)	-10	PDGF BB
CXCR2 (IL-8B) (h) (agonist radioligand)	-1	IL-8
CCR1 (h) (agonist radioligand)	6	MIP-1alpha
H1 (h) (antagonist radioligand)	-7	pyrilamine
H2 (h) (antagonist radioligand)	15	cimetidine
MC4 (h) (agonist radioligand)	7	NDP-alpha -MSH
MT1 (ML1A) (h) (agonist radioligand)	0	melatonin
M1 (h) (antagonist radioligand)	-5	pirenzepine
M2 (h) (antagonist radioligand)	-12	methoctramine
M3 (h) (antagonist radioligand)	6	4-DAMP

M4 (h) (antagonist radioligand)	0	4-DAMP
M5 (h) (antagonist radioligand)	-4	4-DAMP
NK1 (h) (agonist radioligand)	-10	[Sar^{9}, $(Met\ (O_2))^{11}$]-SP
NK2 (h) (agonist radioligand)	-4	[Nleu10]-NKA (4-10)
NK3 (h) (antagonist radioligand)	0	SB 222200
Y1 (h) (agonist radioligand)	-13	NPY
Y2 (h) (agonist radioligand)	-13	NPY
NTS1 (NT1) (h) (agonist radioligand)	-5	neurotensin
delta 2 (DOP) (h) (agonist radioligand)	2	DPDPE
kappa (KOP) (agonist radioligand)	0	U 50488
mu (MOP) (h) (agonist radioligand)	-11	DAMGO
NOP (ORL1) (h) (agonist radioligand)	5	nociceptin
PAC1 (PACAP) (h) (agonist radioligand)	6	PACAP1-38
PPARgamma (h) (agonist radioligand)	0	rosiglitazone
PCP (antagonist radioligand)	4	MK 801
EP2 (h) (agonist radioligand)	0	PGE2
EP4 (h) (agonist radioligand)	3	PGE2
IP (PGI2) (h) (agonist radioligand)	-17	iloprost
P2X (agonist radioligand)	8	alpha ,beta -MeATP
P2Y (agonist radioligand)	13	dATPalpha S
5-HT1A (h) (agonist radioligand)	2	8-OH-DPAT
5-HT1B (antagonist radioligand)	-14	serotonin
5-HT2A (h) (antagonist radioligand)	-2	ketanserin
5-HT2B (h) (agonist radioligand)	-11	(±)DOI
5-HT2C (h) (antagonist radioligand)	-5	RS 102221
5-HT3 (h) (antagonist radioligand)	1	MDL 72222
5-HT5a (h) (agonist radioligand)	-1	serotonin
5-HT6 (h) (agonist radioligand)	-12	serotonin
5-HT7 (h) (agonist radioligand)	11	serotonin
sigma (non-selective) (h) (agonist radioligand)	26	haloperidol
sst (non-selective) (agonist radioligand)	-3	somatostatin-14
GR (h) (agonist radioligand)	-3	dexamethasone
VPAC1 (VIP1) (h) (agonist radioligand)	-9	VIP
V1a (h) (agonist radioligand)	-1	[d(CH2)51,Tyr(Me)2]-AVP
Ca2+ channel (L, verapamil site) (phenylalkylamine) (antagonist radioligand)	1	D 600
KV channel (antagonist radioligand)	0	alpha -dendrotoxin
SKCa channel (antagonist radioligand)	-4	apamin
Na+ channel (site 2) (antagonist radioligand)	1	veratridine
Cl- channel (GABA-gated) (antagonist radioligand)	-2	picrotoxinin
norepinephrine transporter (h) (antagonist radioligand)	2	protriptyline
dopamine transporter (h) (antagonist radioligand)	24	BTCP
5-HT transporter (h) (antagonist radioligand)	-1	imipramine

MMP-1	-3	GM6001
MMP-2	5	GM6001
MMP-3	5	GM6001
MMP-9	10	GM6001

(A)

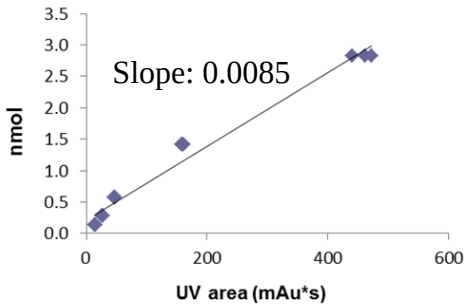

(B)

In Vitro properties	
Log D	2.03
PPB (baboon)	1.4 %
PPB (human)	5.5 %

(C)

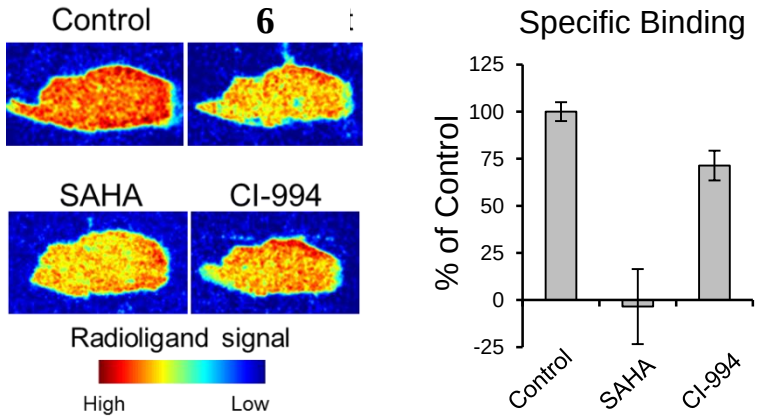

Figure S1. Characterization of [^{11}C]6: *in vitro* properties and *ex vivo* binding.
(A) Mass/UV calibration curve from five concentrations (0.5, 1.0, 2.0, 5.0, 10.0 µM) of standard, unlabeled **6** were made and 100 µL of each concentration were injected in triplicate into analytical HPLC column (UV: 254 nM, Agilent; Gemini C18, 250 x 4.6 mm). The resulting slope was subsequently used to determine the specific activity (moles **6** / radioactivity) of known amounts of prepared [^{11}C]**6**. **(B)** Log *D* and Plasma Protein Binding (baboon and human) were measured with [^{11}C]**6**. **(C)** *Ex vivo* [^{11}C]**6** binding in sagittal rat brain sections. Compared to Control (5% DMSO), radioligand binding is blocked by preincubation with unlabeled **6** or the HDAC inhibitors, SAHA or CI-994 (each at 100 µM) supporting specific binding of **6** to HDAC targets. [^{11}C]-signal not blocked by unlabeled **6** (100 µM) defined nonspecific binding. Specific binding was calculated as (total binding – nonspecific binding) and expressed as % of control in histogram.

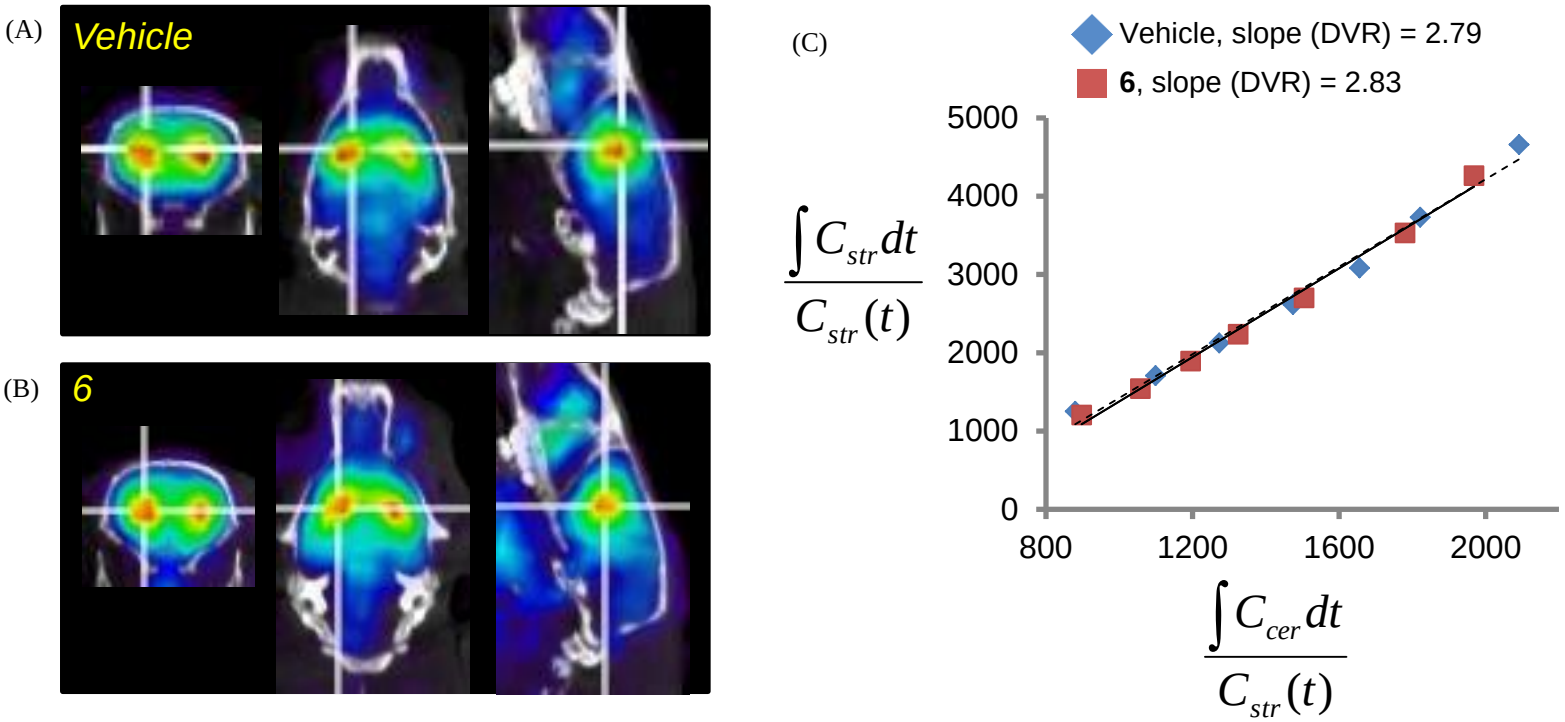

Figure S2: *In vivo* PET imaging confirms acute 6 does not modulate dopamine transporter (DAT) binding/occupancy. The established dopamine transporter (DAT) radiotracer [^{11}C]β-CFT was used to evaluate DAT density/occupancy in rats treated with either (A) vehicle (10% DMSO; 10% Tween 80; 80% saline) or (B) **6** (1mg/kg) via i.p. injection 90 minutes before tracer injection (n=1/group). Dynamic PET imaging was acquired for 60 minutes and resolved uptake of [^{11}C]β-CFT in DAT-rich striatum. Logan distribution volume analysis was conducted for striatum with cerebellum as a reference region, plotted in panel (C), and revealed no impact of 6 treatment on striatal DAT density/occupancy relative to vehicle treated control.

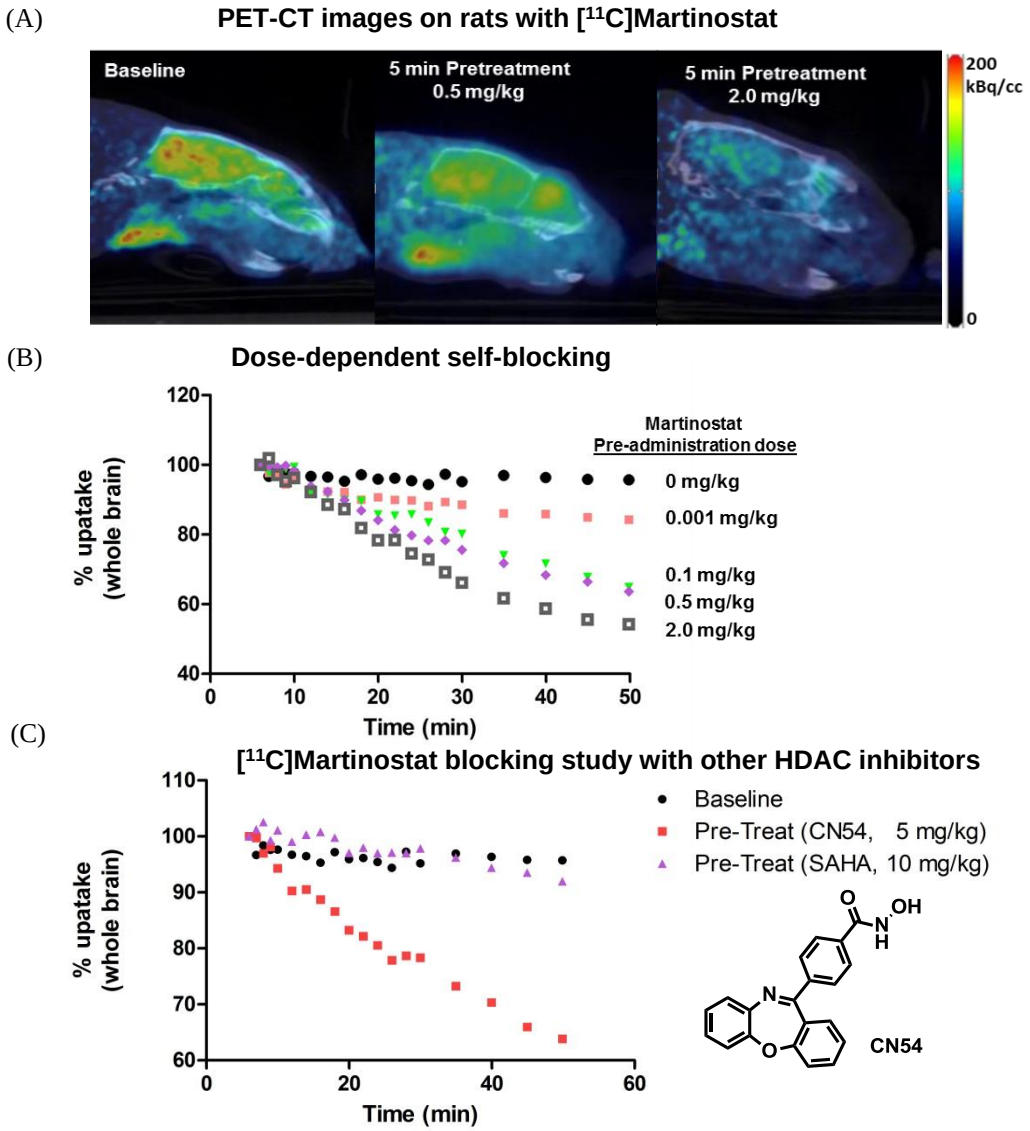

Figure S3. **Rodent *in vivo* PET imaging with [^{11}C]6 reveals robust and blockable uptake in brain.**
(A) Summed PET images (1-60 min) following injection with [^{11}C]**6** at baseline or after pretreatment with 0.5, 1.0 or 2.0 mg/kg unlabeled **6** (self blocking); (B) Whole-brain tracer uptake levels, normalized to uptake at 6min, were altered by 10-40% in self-blocking experiments (pretreatment with 0 - 2.0 mg/kg **6**); (C) [^{11}C]**6** brain uptake was also blocked by 5-min pretreatment with the patent-published HDAC inhibitor CN54 (5mg/kg) but not SAHA (10mg/kg).

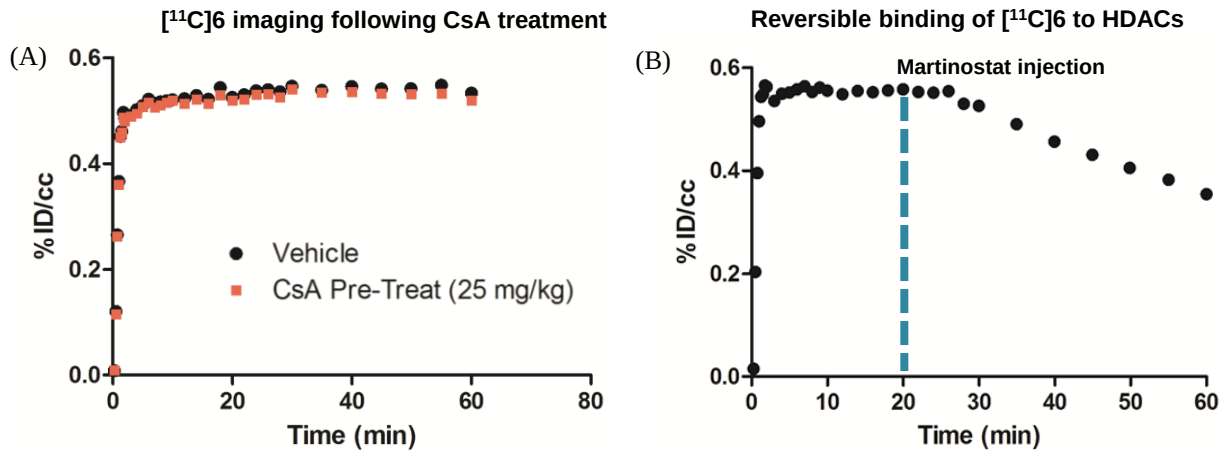

Figure S4. **[^{11}C]6 binding in rat brain is not altered by Pgp inhibition and is reversible.**
(A) Brain uptake of [^{11}C]**6** in rats is equivalent 30 min after pretreatment with vehicle (control) or the P-glycoprotein (Pgp) inhibitor cyclosporin A (CsA, 25 mg/kg, i.v.); (B) Equilibrium binding of [^{11}C]**6** is disrupted by administration of unlabeled **6** (1.0 mg/kg, i.v.) 20 min after tracer injection, demonstrating reversible HDAC binding in brain.

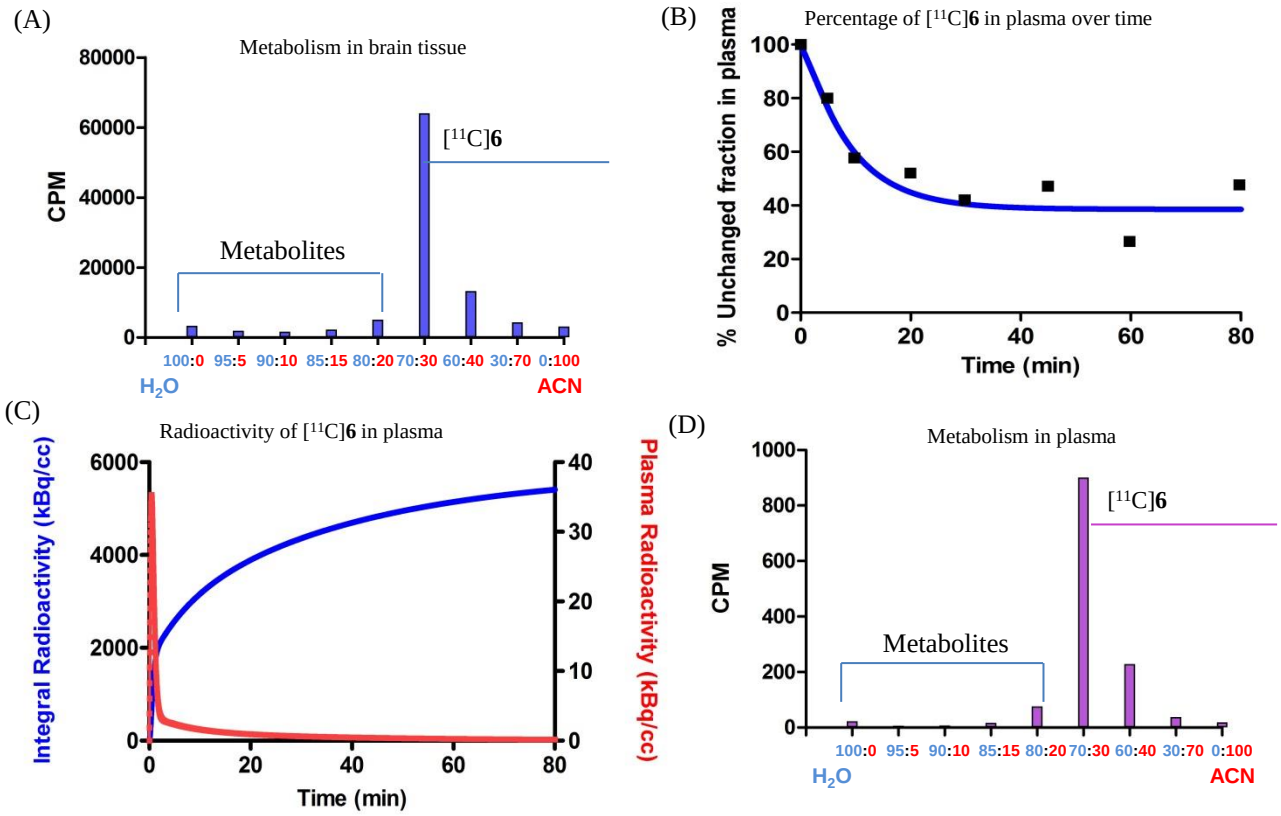

Figure S5. **Radioactive signal from [^{11}C]6 is dominated by lasting presence of parent compound.** (A) Radioactivity in rat brain, 30-min post injection as in (A) demonstrates lasting presence of [^{11}C]**6** in CNS tissue. (B) [^{11}C]**6** stability evaluated in baboon plasma over time showed lasting presence of 40% of parent compound at timepoints >30min. (C) Dual axis plot of baboon plasma analysis shows [^{11}C]**6** radioactivity is rapidly cleared from blood (red, right axis) while metabolite-corrected plasma integral (blue, left axis) demonstrates efficient tracer delivery to perfused tissues. (D) Radioactivity, measured in counts per minutes (CPM), was analyzed in baboon plasma 5-min post injection with [^{11}C]**6**. Minimal radioactivity was detected from polar metabolites eluted with high ratios of water to acetonitrile (ACN).

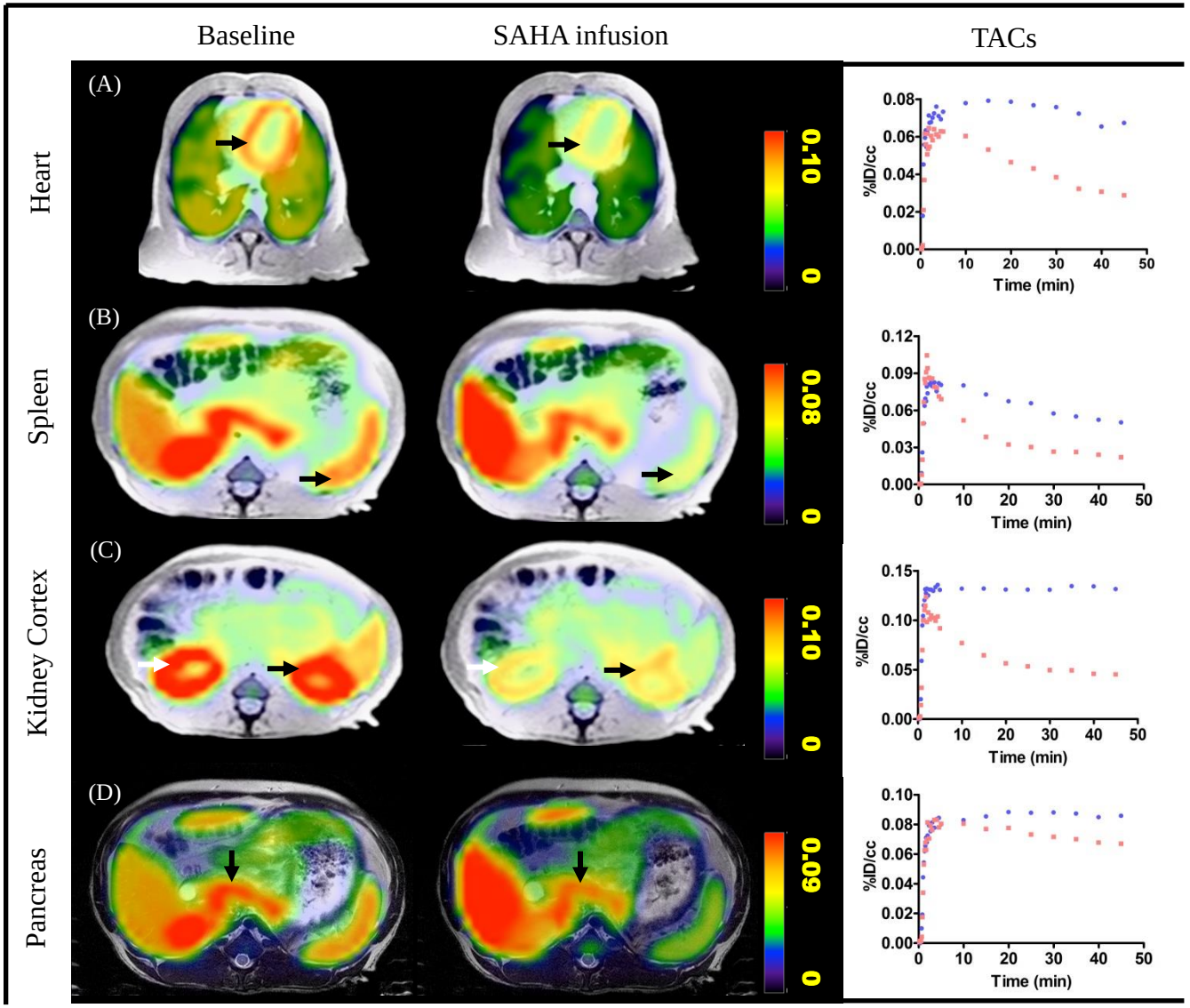

Figure S6. **Organ-specific uptake of [^{11}C]6 in baboon is blocked by SAHA treatment.**
SAHA infusion (2.5 mg/kg/hr, i.v.) was initiated 75 min prior to [^{11}C]**6** administration and continued until the end of PET-MRI imaging (2 hr total). Radiotracer uptake at baseline, visualized in summed images (20-45 min) was reduced by SAHA treatment in organs of interest (arrows) including: A, heart; B, spleen; C, kidney; and D, pancreas. Time activity curves (TACs) show that radiotracer uptake at baseline (blue) was reduced by SAHA infusion (red). SAHA-induced displacement of [^{11}C]**6** resulted in elevated tracer levels in liver, (B, D) an expected effect due to normal metabolic function.